npj | climate and atmospheric science

www.nature.com/npjclimatsci

ARTICLE OPEN

Check for updates

Delayed coastal inundations caused by ocean dynamics post-Hurricane Matthew

Kyungmin Park[1]✉, Emanuele Di Lorenzo[2], Yinglong J. Zhang[3], Harry Wang[3], Tal Ezer[4] and Fei Ye[3]

Post Hurricane Abnormal Water Level (PHAWL) poses a persistent inundation threat to coastal communities, yet unresolved knowledge gaps exist regarding its spatiotemporal impacts and causal mechanisms. Using a high-resolution coastal model with a set of observations, we find that the PHAWLs are up to 50 cm higher than the normal water levels for several weeks and cause delayed inundations around residential areas of the U.S. Southeast Coast (USSC). Numerical experiments reveal that while atmospheric forcing modulates the coastal PHAWLs, ocean dynamics primarily driven by the Gulf Stream control the mean component and duration of the shelf-scale PHAWLs. Because of the large spatial impact of the post-hurricane oceanic forcing, the coastal hazards are not limited to a direct hit from a hurricane but can be detected throughout the USSC where the oceanic processes reach.

npj Climate and Atmospheric Science (2024)7:5 ; https://doi.org/10.1038/s41612-023-00549-2

INTRODUCTION

Flooding poses the most destructive threat to coastal communities and is projected to worsen in response to climate-related sea level rise, higher precipitation, and more powerful and frequent hurricane events[1,2]. The predominant focus for the impacts of hurricanes has been on the influence of storm surge[3–7], wind wave[8–10], precipitation[11] and river discharge[12,13]. However, persistent abnormal water levels, adding to the delay in the restoration of flood damage by the storm surge, have also been observed during the post-hurricane period as a result of the influence of the oceanic dynamic adjustment[14–16]. Hurricane Matthew (2016) provides clear evidence of persistent abnormal water levels after the hurricane leaves the U.S. Southeast Coast (USSC). Figure 1 shows the track and intensity of Matthew and the time series of Non-Tidal Residual Anomalies (NTRAs) from the eight NOAA tide gauges along the USSC. In the post-hurricane period, the maximum NTRAs at each station range from 35 to 50 cm, and positive NTRAs last from several days to weeks. The magnitude and duration pose long-lasting threats to coastal communities in the form of nuisance flooding[17]. However, the previous modeling and observational studies (reviewed next) have not thoroughly examined the oceanic adjustment dynamics that lead to sustained high sea levels following the hurricane forcing. Therefore, improving our knowledge to analyze and predict the abnormal water level during and after hurricanes holistically is a critical step for better planning of coastal protection and conservation strategies.

Different oceanic processes affecting coastal sea levels along the USSC can be summarized as follows. Domingues et al.[18] reported that accelerated sea level rise in the USSC during 2010–2015 was driven by warming of the Florida Current (FC) upstream of the Gulf Stream (GS). Specifically, they attributed the sea level rise of 12.5 cm on the Florida coast to the thermostatic contribution during 2010–2015. Volkov et al.[19] proclaimed that the ocean heat component associated with Atlantic Meridional Overturning Circulation (AMOC) is linked to interannual sea level changes along the coastline of the South Atlantic Bight (SAB). Furthermore, using multi-decadal observations, Volkov et al.[20]. showed that the thermostatic sea level rise associated with AMOC had a significant influence on the frequency of coastal floods in the USSC. In addition, hurricane forcing can remarkedly affect large-scale ocean circulations such as the GS, which in turn plays a critical role in modulating coastal sea levels. Historically, when hurricanes pass near the GS, significant weakening of the western boundary current has been observed, for example, during Hurricanes Bill (2009: Kourafalou et al.[21]), Joaquin (2015; Ezer and Atkinson[22]) and Dorian (2019; Park et al.[15]; Ezer et al.[23]). During the passage of Matthew, observations and models also show significant decreases in the intensity of the GS by up to 50%[15,24]. The weakening of the GS associated with the variations in the sea levels follows the context of geostrophic balance. Several studies have provided evidence for the role of the GS in influencing coastal sea levels using the measurement of the FC at Florida Strait between Miami and the Bahamas[3,23,25,26,27]. During the period from 1960 to 2012, Dangendorf et al.[28] showed high correlations between coastal sea levels and the GS pathway in the USSC, implying the fast barotropic response of the water levels to the characteristics of the GS. The planetary oceanic waves have also played important roles in coastal sea levels. For instance, it is found that long-term (e.g., multi-decadal scale) variation in coastal sea levels along the USSC are correlated with the wind-driven basin-wide Rossby wave that propagates westward from the open ocean (Calafat et al.[29]; Dangendorf et al.[30]). When hurricanes travel along the continental shelf in the SAB (e.g., Matthew, 2016), positive sea level anomalies remain around Cape Hatteras (e.g., north of the USSC) following the departure of the hurricane from the coast. The oceanic adjustment to the anomalies can cause Coastally Trapped Waves (CTWs) to propagate cyclonically along the coastlines (e.g., southward on the western boundary in the North Atlantic Ocean) due to the geostrophic dynamic, and the CTWs modulate coastal sea levels[31]. While the CTWs were reported to travel northward along the USSC due to the GS in

[1]Coastal Sciences Division, Pacific Northwest National Laboratory, Seattle, WA 98109, USA. [2]Department of Earth, Environmental and Planetary Sciences, Brown University, Providence, RI 02912, USA. [3]Virginia Institute of Marine Science, College of William & Mary, Gloucester Point, VA 23062, USA. [4]Center for Coastal Physical Oceanography, Old Dominion University, Norfolk, VA 23508, USA. ✉email: kyungmin.park@pnnl.gov

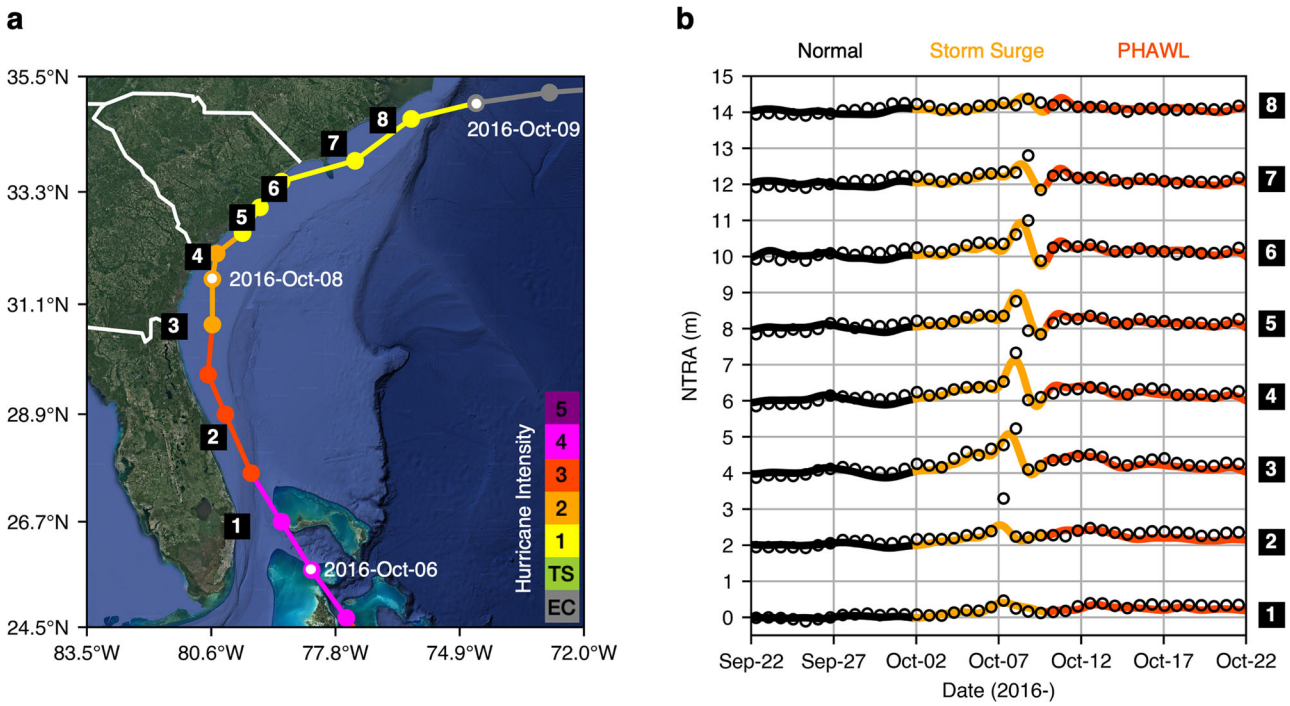

Fig. 1 Hurricane characteristics and PHAWL. a Hurricane track and intensity of Matthew (2016) and locations of selected NOAA tide gauges (black square with numbers). **b** Time histories of NTRAs from the selected NOAA tide gauges. The NTRAs are relative NTR to the mean water levels during the normal period (2016-Sep-01 to 2016-Oct-02) at each NOAA tide gauge. The numbers inside the square correspond to the stations' numbers in (**a**). The open circles represent the NTRAs from the developed numerical model.

the past[32], recent studies have provided evidence of southward CTWs along the coast using numerical models and observations. For example, Ezer[33] detected CTWs propagating from north to south of Cape Hatteras using NOAA tide gauges and numerical simulations although the characteristics of the CTWs change south of Cape Hatteras. Using observations, Pujiana et al.[34] also found subseasonal (e.g., 20 ~ 100 days) CTWs propagating southward along the USSC with an amplitude of up to 15 cm.

Despite the previous works aforementioned, there are still knowledge gaps regarding the spatiotemporal scales and causal mechanisms for abnormal water levels during post-hurricane conditions. For example, the impact of the Rossby waves on coastal sea levels cannot reasonably explain the high-frequency post-hurricane ocean dynamics because the Rossby waves have a long timescale (longer than months). The thermostatic contribution from large-scale ocean circulation is not expected to cause an abnormal increase in water levels during post-hurricane events because of the significant cooling impact of hurricanes. While the CTWs have been studied for subseaonal to decadal scale, high-frequency CTWs, particularly during the post-hurricane period, have yet to be studied thoroughly. Besides, Ezer[33] examined the impact of the GS on water levels using a model with an imposed, artificially varying transport of the GS through the open boundary condition rather than considering the interactions of the GS with the hurricane itself. Thus, these findings do not thoroughly explain the short-term behavior of the oceanic drivers in the post-hurricane period (e.g., hours to days). In addition, previous efforts by Ezer and Atkinson[22] only consider the characteristics of the GS limited to locations where available observation exists (e.g., at Florida strait), and therefore do not resolve the spatially varying characteristic of the GS, which leads to weak correlations between the GS transport measured at the Florida strait and the sea levels along the USSC coast (e.g., R^2 of 0.04–0.16). Chi et al.[35] also emphasized the importance of the GS transport measurement at multiple locations to properly understand the relation between the GS and sea levels by showing different correlation patterns between the north and south of Cape Hatteras. However, as Chi et al.[35] used monthly-mean measurements that could not capture the higher-frequency variations of the GS and those of the sea levels, the study is limited to explaining the abnormal water levels associated with the ocean dynamic during the post-hurricane period[36]. Other studies based on the tide gauges that aim at inferring the relationship with the GS can also cause poor correlation with the GS because the water levels at the tide gauges are affected not only by the large-scale ocean circulation but also by local wind stress, air pressure, surface waves and other ocean dynamics[37,38]. In order to reproduce the temporal and spatial variations of the total water level driven by various coastal ocean dynamics, numerical models remain to be unique and indispensable tools, despite challenges of its own such as coarse model resolution (by global ocean reanalyses), lack of 3D baroclinic dynamics (for 2D coastal flooding models), and the presence of ocean mixing errors[15,39,40].

In this study, we use a high-resolution, 3D unstructured grid, baroclinic coastal ocean model (see Methods) to simulate the spatial and temporal extent of the PHAWL over the entire SAB during and after Hurricane Matthew in 2016. The comparison of the model results with observations yields excellent skills and shows that the model is capable of capturing not only the persistent PHAWL (Fig. 1b) but also storm surges, the GS, and the large-scale ocean fields (as shown in Supplementary Figs. 2–8). We then proceed to use the model to conduct a series of sensitivity numerical experiments to quantify the relative roles and contributions played by each of of key drivers in generating PHAWL. We find that while atmospheric forcing controls the fluctuation components of the coastal PHAWL, oceanic dynamics predominantly driven by the GS determine the mean components of shelf-scale PHAWLs.

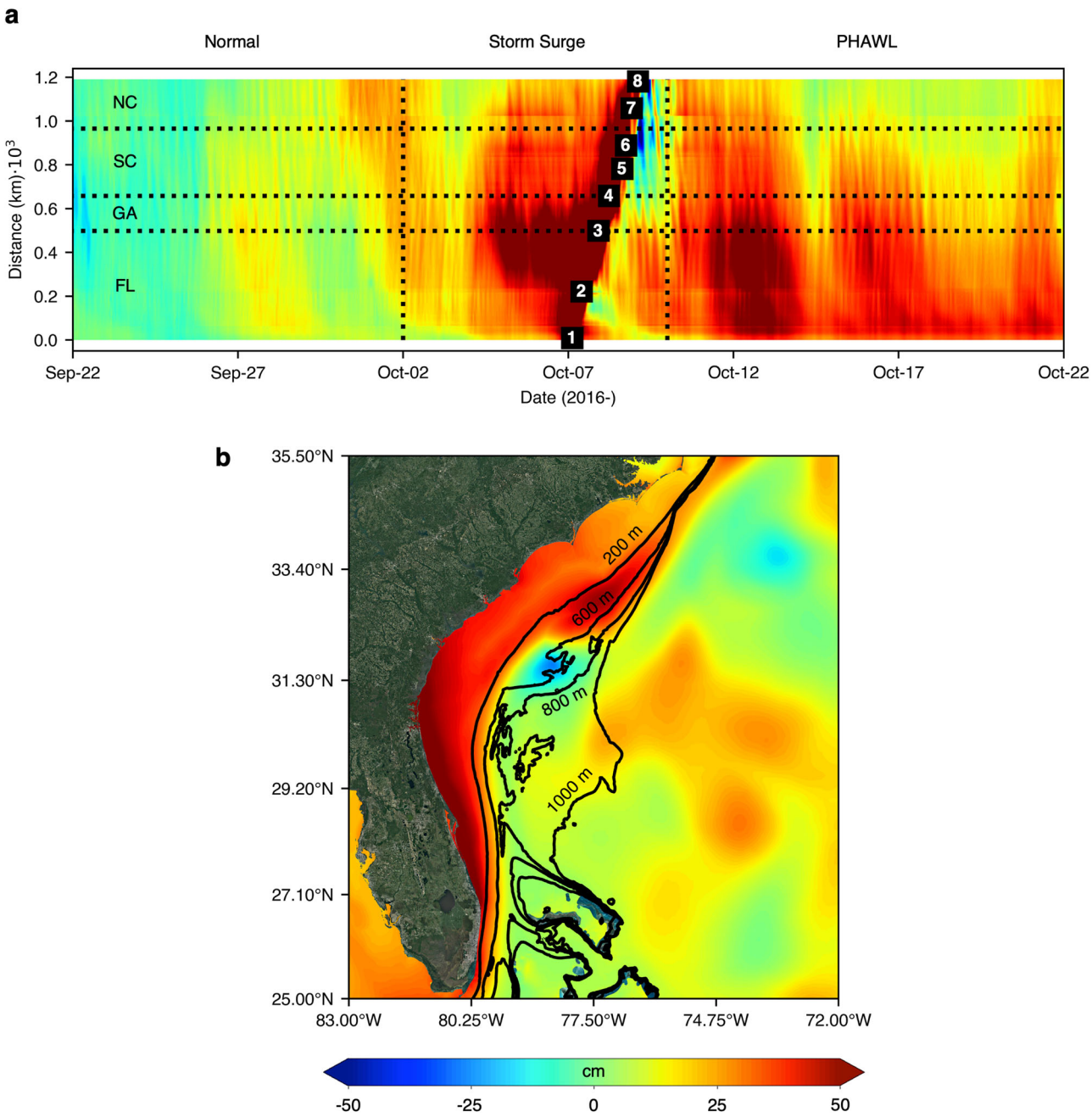

Fig. 2 Spatiotemporal impact of the PHAWL. a Hovmöller diagram of modeled NTRAs (cm) along the USSC. The black squares with numbers correspond to the peak timing of storm surges at each NOAA station presented in Fig. 1a. **b** Modeled maximum NTRAs (cm) in the post-hurricane event (2016-Oct-11 to 2016-Oct-22). The solid black lines indicate isobaths of 200, 600, 800 and 1000 m. The NTRAs in (**a**) and (**b**) are relative non-tidal residuals to the mean water levels in the normal period (2016-Sep-01 to 2016-Oct-02) at each grid point. a and b share the same color bar.

RESULTS

Spatiotemporal impacts of the PHAWL

Since high-frequency measurements of water levels (e.g., 6 min sampling from NOAA tide gauges) are limited to the coastline, we utilize a high-resolution coastal ocean model (see Methods) to further analyze the spatiotemporal pattern of the PHAWL in the SAB. The Hovmöller diagram in Fig. 2a shows the modeled NTRAs along the USSC as a function of time (*x*-axis) and distance (*y*-axis) from the Florida (FL) coast to the North Carolina (NC) coast. The black squares with the numbers in Fig. 2a represent the peak timing of the NTRAs at each NOAA tide gauge indicated in Fig. 1b. The Hovmöller diagram clearly shows the progression of the storm surges from FL to NC coasts between 2016-Oct-07 and 2016-Oct-09, which is associated with the direct impact of Hurricane Matthew. Following the departure of the hurricane from the NC coast on 2016-Oct-10, the high PHAWLs ranging from 20 cm to 54 cm hit the entire SAB coast until 2016-Oct-14. After that, the magnitudes of the coastal PHAWLs fluctuate over time. The PHAWLs decrease up to 10 cm on the NC coast, while high PHAWLs (45 cm) remain on the FL coast until 2016-Oct-22. In Fig. 2b, the 2-D map of the maximum NTRAs in the post-hurricane period shows the spatially varying magnitude of the peak

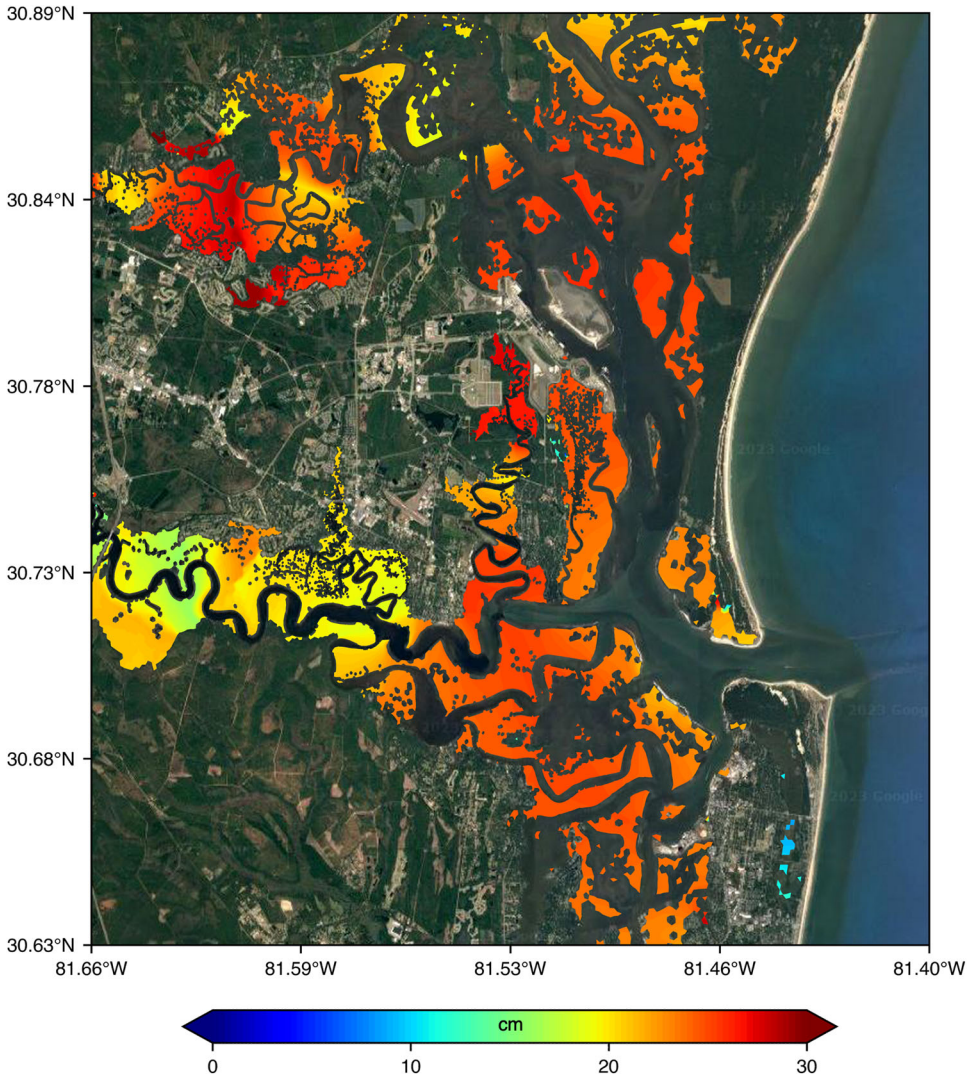

Fig. 3 Impacts of the PHAWLs on inundation depths. The difference in the maximum inundation depths (cm) between the normal (2016-Sep-01 to 2016-Oct-02) and post-hurricane periods (2016-Oct-10 to 2016-Oct-22) in the south GA coast. The inundation depth represents the total water level above ground during each period.

PHAWLs. Noticeable peaks with magnitudes of 20–58 cm spread from the shelf break (the isobath of 200 m) to the coastlines, which implies the tight coupling of the near coast and shelf dynamics. The tight coupling mechanism in the cross-shelf scale is further discussed in the following section. The high peak PHAWL values (e.g., above 50 cm) are distributed in the southern part of the SAB continental shelf, predominantly in the south Georgia (GA) and FL coasts. The results exhibit persistent PHAWL affecting the entire SAB coast with increased water levels of up to 58 cm compared to normal conditions. In particular, the southern parts of the USSC pose the highest vulnerability to the abnormal water levels in the post-hurricane period.

We further leverage the developed model to investigate the impact of the PHAWLs on coastal flooding in a community area. We implement a city-grid-scale model (see Methods) on the south GA coast to simulate coastal inundation in the cities and the surrounding coastal plain. The south GA coast was selected because it is an area characterized by complex wetland morphologies and it exhibits one of the highest PHAWLs along the USSC, as shown in Fig. 1b (NOAA station 3) and in Fig. 2. The inundation map from the model in Fig. 3 shows the noticeable impact of the PHAWL on the inland portion of the coastal zone. The PHAWLs increase the inundation depths by up to 30 cm in wetlands and residential areas. The high-resolution model results emphasize the significant impact of the persistent abnormal water levels even after the hurricane event, which can hamper post-storm restoring efforts and pose an additional threat to coastal communities in the form of nuisance or sunny day flooding.

Main drivers of the PHAWL

Leveraging a well-verified numerical model with observations (Supplementary Figs. 2–8), we conduct numerical experiments to investigate the relative roles and contributions of the main drivers in generating the PHAWL. In the numerical experiments, the control run (CTRL) includes all forces (e.g., precipitation, wind, air pressure, heat flux, and oceanic forcing) and represents the original PHAWL. The key drivers are categorized as ATmospheric Forcing (ATF) and OCeanic ADJustment (OCADJ), which are identified distinctly through numerical experiments (see Methods). Because the main forces contribute differently to the PHAWL, identifying the dominant driver reveals key information on the underlying mechanisms of the PHAWL. Figure 4a shows water levels caused by different main drivers along the SAB coastline.

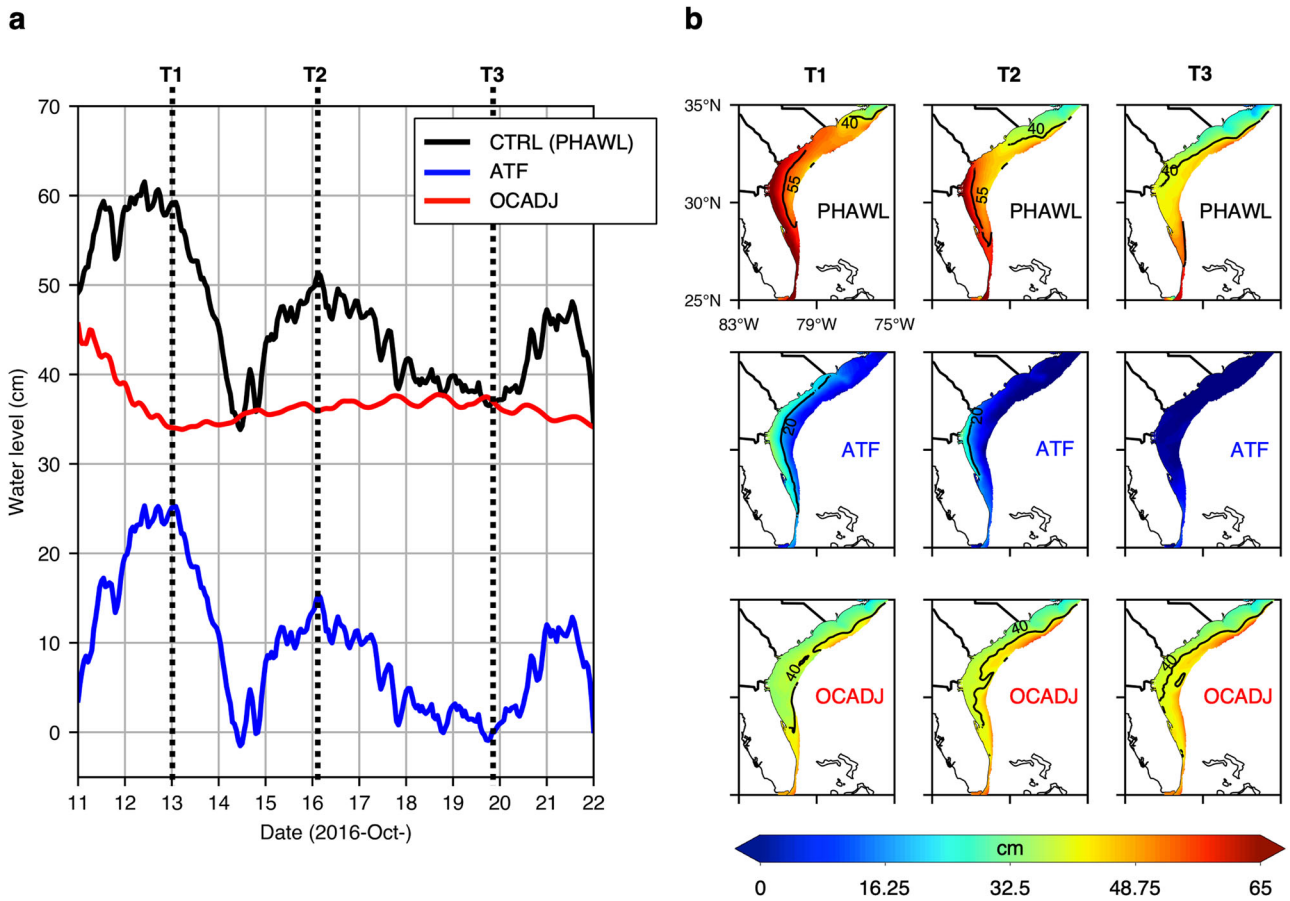

Fig. 4 Relative roles and contributions of main drivers. a Time histories of mean water levels (cm) along the coastlines in the SAB. The line colors indicate the main drivers such as all forcing (CTRL; black), atmospheric forcing (ATF; blue) and oceanic adjustment (OCADJ; red). **b** Instantaneous fields of the water levels (cm) on the SAB continental shelf at the times of T1 (Oct 13 00:00:00 in the first column), T2 (Oct 16 02:00:00 in the second column) and T3 (Oct 19 22:00:00 in the third column) that are indicated in (**a**). The continental shelf is an area with water depths below 200 m.

The ATF-induced water level (blue line in Fig. 4a) has a time-varying magnitude depending on wind and air pressure conditions. The highest water level caused by ATF is observed on 2016-Oct-13 with a magnitude of 25 cm, which takes 42% of the PHAWL. After the peak, the ATF-induced water level fluctuates from −1 to +15 cm. The water level caused by OCADJ spikes to the highest level (45 cm) at an early stage of the post-hurricane period (2016-Oct-11), accounting for more than 90% of the PHAWL. The CTW plays a critical role in the peak level during that period, which is covered in more detail in the next section. After the CTW event, the OCADJ keeps the high water level with magnitudes of 33–38 cm throughout the ten days and therefore determines the mean component of the PHAWL. In Fig. 4b, we further analyze the spatiotemporal evolution of the PHAWL on the SAB continental shelf. From a spatial point of view, we find that the PHAWL is characterized by the main signals consisting of one along the coast and another emanating from the shelf break, which is clearly found at T1 (Oct 13), T2 (Oct 16), and T3 (Oct 19) in Fig. 4b. The coastal signals of PHAWL at the T1 and T2 are pronounced by the ATF because the forcing increases the coastal sea levels by up to 35 cm at T1 and 28 cm at T2, as shown in the second row of Fig. 4b. Note that the impacts of the ATF are limited to the vicinity of the coast because the wind stress has more pronounced influence on the shallower water[41]. Accordingly, the impacts of the ATF on offshore water levels around the shelf break are relatively minor. When the ATF is weak at the T3 (third column in Fig. 4b), the PHAWL shows the cross-shore gradient of the water levels, namely high offshore water levels and low coastal water levels due to the OCADJ. The third row in Fig. 4b shows that the OCADJ controls the offshore signals entering through the shelf break, which gradually grow and propagate into the coast. The offshore water levels along the shelf break increase over time to reach up to 52 cm. With the amplified offshore signals, the coastal sea levels induced by OCADJ increase to 25 ~ 43 cm depending on locations where the FL coast has the highest increase in the water level due to the OCADJ. In quantifying the relative role and contribution of the primary drivers on different spatiotemporal scales, we argue that the ATF controls the fluctuation component of the coastal PHAWL (e.g., fluctuations of the PHAWL along the SAB coast in Fig. 2a), while the OCADJ is a key component in determining the magnitude and duration of the shelf-scale PHAWL.

Characteristics of post-hurricane OCADJ

Understanding the true nature of the OCADJ is crucial to identify the mechanism of the shelf-scale PHAWL. We find two distinct oceanic processes during the post-hurricane period. First, fast alongshore signals are observed in the form of CTWs following the departure of Hurricane Matthew. After Matthew leaves the Cape Hatteras (the northern part of the SAB) on 2016-Oct-10, the positive Sea Surface Height Anomalies (SSHAs) remain in the area as presented in Fig. 5a. As the pressure gradient caused by the SSHAs is balanced by the Coriolis force (e.g., geostrophic

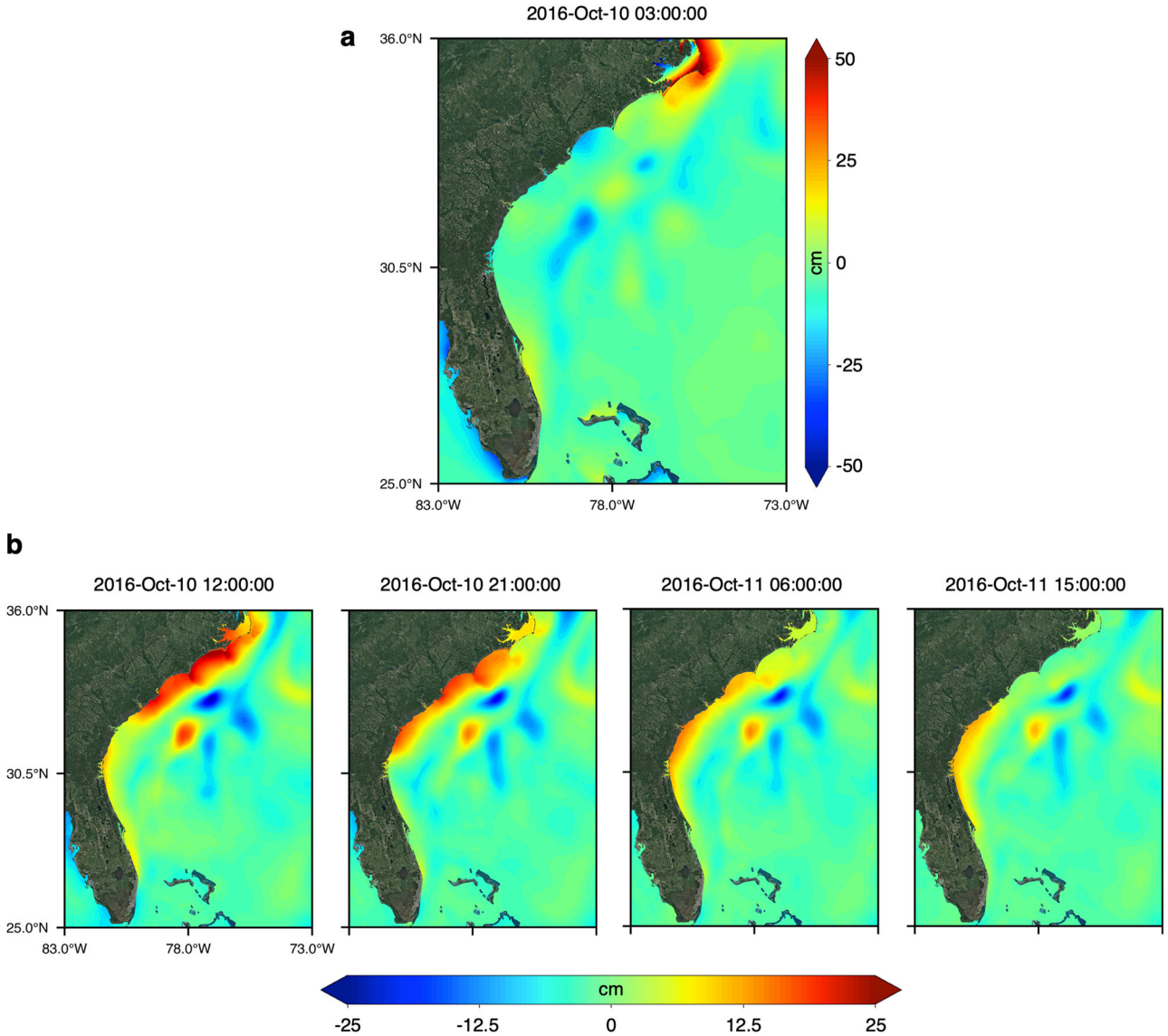

Fig. 5 CTWs after Hurricane Matthew. a Snapshot of modeled sea surface height anomalies (cm) from the CTRL experiment after Hurricane Matthew leaves the North Carolina coast (e.g., 2016-Oct-10). **b** Time-sequence maps of OCADJ-induced SSHAs (cm).

dynamic), the high sea level propagates cyclonically from the north toward south along the SAB coastline. The snapshots in Fig. 5b clearly show the fast propagation (~12 m s^{-1}; which corresponds to the speed of a shallow water wave) of the OCADJ-induced SSHAs at the early stage of the post-hurricane period. Although NOAA tide gauges with a 6-min sampling interval can capture the high-frequency signals of the CTWs, it is difficult to isolate the CTWs from the measurements where different frequencies of signals are embedded such as wind-, air pressure-, and tide-driven signals. However, the fast propagation of the CTWs in Fig. 5 is comparable with the findings of the previous study that utilized numerical simulations[33]. The characteristics of the CTW also resemble the observed and theoretical subseasonal (20 ~ 100 days) waves flowing along the SAB coastline[34]. Pujiana et al.[34] categorize the subseasonal CTWs into continental shelf waves and Kelvin waves based on dispersion relation with daily measurements of water levels from tide gauges and satellites. They reported that the CTWs in the Florida Strait can be expressed as Kelvin waves with a speed of 7.7 m s^{-1} while the continental shelf waves are observed between the NC (Duck Pier in North Carolina) and SC (Charleston in South Carolina) coasts with a speed of 9 m s^{-1}. As a result, we attribute the dominant source determining the initial peak of the OCADJ-induced water level to the CTWs, as shown in Fig. 4a.

Another important oceanic process is a cross-shore signal entering from the shelf break, which significantly contributes to the long-lasting shelf-scale PHAWL. Since the shelf break from which the high-water levels propagate is close to the GS, a question arises as to whether the water level dynamics are driven by the large-scale ocean circulation. To explain the relationship between the GS and the offshore signals, we utilize the correlation map in Fig. 6a, showing pointwise correlations between the GS intensity and water levels from CTRL in the period of 2016-Sep-22 to 2016-Oct-22. Figure 6a presents strong anticorrelations on the continental shelf as the west side of the GS. In particular, high correlations ranging from −0.88 to −0.7 are observed around the shelf break, which implies a crucial role of the GS in the offshore signals in Fig. 4b. The negative relationship in the continental shelf means that the weaker GS results in higher water levels on the shelf, which is valid in the context of geostrophic balance[25,42]. This

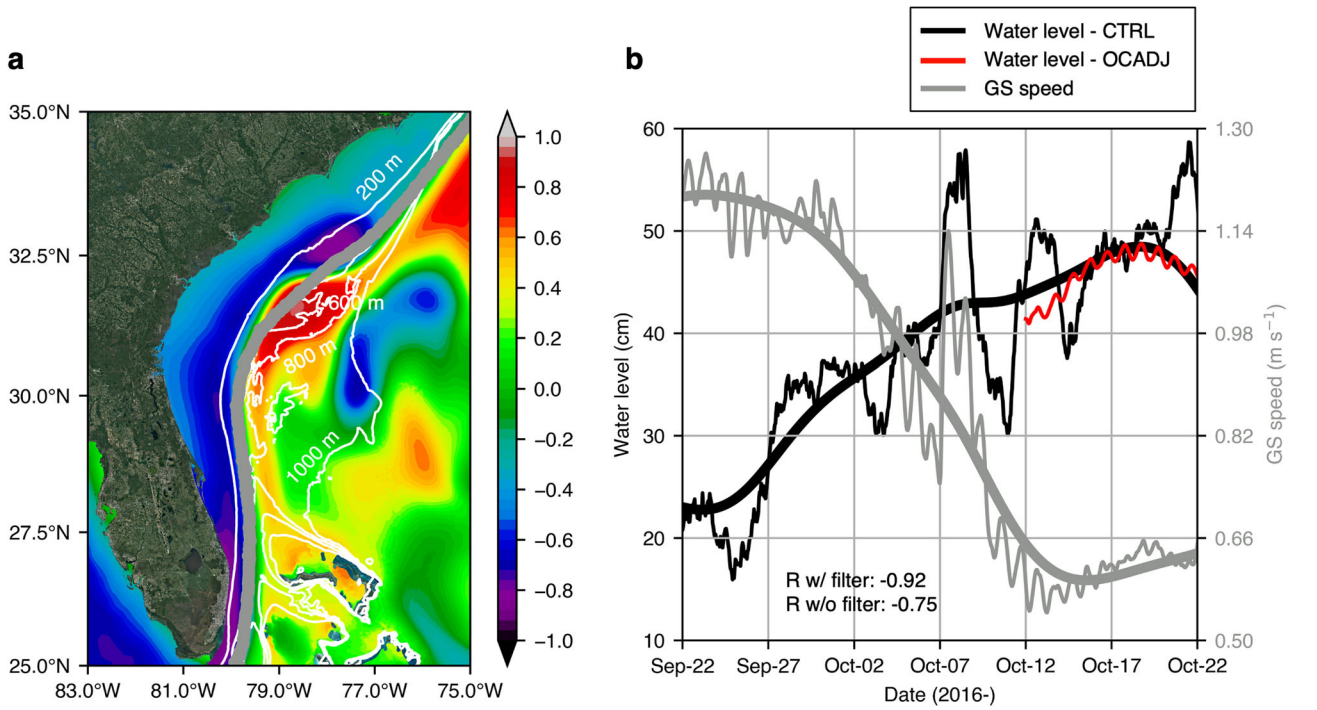

Fig. 6 The GS-generated offshore signals. a Correlations between the GS speed and water levels at each grid point in the period of 2016-Sep-22 to 2016-Oct-22. The GS speed is the mean ocean current speed along the GS's path (thick gray line). The white lines represent the isobath of 200, 600, 800, and 1000 m; the shelf break is the isobath of 200 m. **b** Time histories of the GS speed from CTRL (gray line; m s^{-1}) and the mean offshore water levels along the shelf break from CTRL (black line; cm) and OCADJ (red line; cm). The thick lines indicate the low-pass filtered signals. The Rs are correlation coefficients between mean GS speed and water level for the signals with and without low-pass filter.

explains how the change in the GS during Hurricane Matthew results in the PHAWL. Figure 6b presents the time histories of the mean current speed along the GS path (gray line) and mean water level along the shelf break (black line). The low-pass filtered variation of the CTRL-generated water level (thick black line) reflects the influence of the OCADJ on the water level (red line) because the two signals have similar temporal evolution and magnitude in Fig. 6b. The GS speed decreases by up to 50% due to the combination of hurricane mixing and the winds countered to the GS's direction[14], while the offshore water levels along the shelf break increase in accordance with the weakening of the GS. The intensity reduction of the ocean circulation is also verified by the submarine cable measurement at the Florida Strait (Supplementary Fig. 5). The result underpins the important role of the GS in generating the offshore signals propagating across the shelf. It should be noted that since the Florida coast is closer to the shelf break, the higher correlations (−0.85 to −0.47) are found around the Florida coast compared to other coasts (−0.45 to −0.17) in the SAB, which means that the FL coast is more vulnerable to the GS changes. The geographical characteristic (i.e., proximity to the shelf break) significantly contributes to the long-lasting elevated PHAWL on the FL coast, as emphasized in Fig. 2. In summary, CTW and GS were identified as the two key processes driving the shelf-scale PHAWL during the post-hurricane oceanic adjustment. The CTW causes fast alongshore modulation of coastal sea levels on the time scale of 1 ~ 3 days, while the GS leads to persistent cross-shore signals on the time scale over 10 days in the entire continental shelf.

DISCUSSION

Leveraging the 3D, high-resolution, baroclinic coastal ocean model in combination with the observation from NOAA's tide gauges, we examine the persistent abnormal water level dubbed "PHAWL" during the post-hurricane Matthew period. As shown in the city-block scale numerical model results, the increased inundation depth can go up to 30 cm around residential areas due to the PHAWL. This highlights the need for integrated coastal emergency response plans not only during the time of direct hit by a hurricane (e.g., storm surges and heavy precipitation) but also for the post-hurricane phase when the restoration is urgently needed. Through numerical experiments, we identify the dominant mechanism for the persistent shelf-scale PHAWL to be the CTW and the signal from GS as part of the oceanic adjustments. During the initial adjustment stage, the fast coastal signals caused by CTWs (on the time scale of 1–3 days) create spikes in water levels along the USSEC, whereas in the later stage, the GS-generated cross-shore signals (on the time scale over 10 days) determine the mean component of the PHAWL over the entire continental shelf. The large-scale impacts mean that the coastal hazards are not limited to the hurricane's landfall location but can be detected at any location where the oceanic processes can reach.

Our results suggest that future coastal modeling frameworks used for addressing the flooding dynamics should consider not only atmospheric forcing but also oceanic adjustment processes to provide a robust prediction of total water levels and inundations. Given the projection of more frequent and powerful hurricanes under climate change, the inclusion of oceanic responses (with the presence of large-scale ocean circulations) associated with hurricane forcing is especially important, which will contribute to a better understanding of the underlying mechanisms for coastal flooding.

Further studies with different hurricane characteristics are required to clarify and quantify the impacts of the oceanic adjustments on the PHAWL. Considering the important role of the GS in determining the PHAWL, the magnitude and duration of the PHAWL can heavily rely on hurricane tracks and intensities that have a strong influence on the large-scale ocean circulation. For example, Hurricane Matthew targeted in this study traveled near the GS (e.g.,

shore-parallel track) and then weakened the GS significantly during the passage, which would cause significant PHAWL. The question arises whether other hurricanes with different tracks and intensities have a similar impact on the GS and cause PHAWL as Matthew does. Therefore, future studies should utilize ensemble experiments with historical or synthetic hurricanes to assess the statistical nature of the ocean dynamics related to hurricanes.

METHODS

3-D baroclinic coastal ocean model

To simulate 3-D baroclinic ocean dynamics and their impact on coastal sea levels along the U.S. southeast coast, we use the Semi-implicit Cross-scale Hydroscience Integrated System Model (SCHISM) which has been extensively validated from city-block scale to global-scale simulations (Zhang et al.[43]; Ye et al.[44]; Huang et al.[45]). The grid system of the model covers the entire U.S. east coast and the Gulf of Mexico in the longitude range of 98°W and 60°W and the latitude range of 8°N and 46°N. The resolutions of the horizontal grid range from 6 km (open ocean) to 5 m (inland region) using an unstructured grid. The high-resolution (~5 m) is applied to the south Georgia coast where Hurricane Matthew caused the highest storm surge and PHAWL among the coastal cities in the U.S. southeast coast. Correspondingly, the inland rivers and lands are properly resolved to simulate and analyze inland flooding caused by the PHAWL on the Georgia coast while we include only the coastlines in other regions to reduce computational costs in this study. The Digital Elevation Model (DEM) of the General Bathymetric Chart of the Oceans (GEBCO) 2022 is used for the model bathymetry in the open ocean while the high-resolution DEM from the Continuously Updated Digital Elevation Model (CUDEM) is utilized for the inland topobathymetry in the Georgia coast. The number of layers in the vertical grid varies with bathymetries to take full advantage of the polymorphism (e.g., a single grid system can seamlessly morph among full 3D, 2D depth-averaged, 2D laterally averaged and quasi-1D configurations; Zhang et al.[43]). We combine the two atmospheric models such as European Centre for Medium-Range Weather Forecasts (ECMWF) and High-Resolution Rapid Refresh (HRRR) for the surface forcing, while Copernicus Marine Environment Monitoring Service (CMEMS; for water temperature, salinity, and velocity) and Archiving, Validation, and Interpretation of Satellite Oceanographic data (AVISO; for sea surface height) are utilized for the initial and boundary conditions of the model. For the simulations of total water levels with tides and coastal inundations, we use FES 2014 to specify eight major tidal constituents (K1, K2, M2, N2, O1, P1, Q1, and S2) on the open boundary and the tidal potentials in momentum equations. The simulation of the total water level under the realistic forcing allows us to estimate the inundation depths above ground (e.g., Fig. 3). The entire simulation period is 90 days, from 2016-Aug-1 to 2016-Oct-31, focusing on Hurricane Matthew and the post-hurricane period from 2016-Sep-28 to 2016-Oct-22.

We have utilized extensive observations such as NOAA tide gauges, submarine cable, Argos, AVISO and JPL- Group for High Resolution Sea Surface Temperature (GHRSST) to validate model results such as coastal sea levels, Gulf Stream (e.g., path and intensity), 3-D ocean temperature and salinity. The good agreements between the observations and models are presented in Supplementary Figs. 2–8. We, therefore, have confidence in the capability of the model to capture the key ocean processes that control the coastal dynamics and the sea level change during the post-hurricane period.

Sensitivity experiment

Numerical experiments are conducted to provide better insight into the mechanism of the PHAWL in the period of 2016-Oct-11 to 2016-Oct-22. We separate the drivers into two main categories, ATmospheric Forcing (ATF) and OCeanic ADJustment (OCADJ) through a set of sensitivity simulations. To focus on the impact of the main drivers, we extract the tidal signals from the open boundary condition and body force in momentum equations in each experiment. The first experiment, referred to as the control run (CTRL), represents the 3-D baroclinic simulation with all forcing (e.g., precipitation, wind, air pressure, heat flux and oceanic forcing). The second experiment excludes the atmospheric forcing (e.g., wind stress, air pressure, heat flux and precipitation) from CTRL, which is named OCADJ hereafter. Accordingly, the OCADJ represents ocean dynamics during the post-hurricane period, which is not affected by atmospheric forcing. Using the difference between the CTRL and OCADJ outputs, we isolate the impact of atmospheric forcing on water levels, which is referred to as ATF. Note that the dataset obtained from the difference between experiment outputs can include minor nonlinearity. For example, nonlinear interaction between atmospheric forcing and oceanic adjustment can be included in the ATF as a non-oceanic forcing residual. With these definitions, the CTRL simulation corresponds to the original PHAWL and is identical to the summation of the ATF and OCADJ (e.g., closed sea level budget). With the new dataset from the numerical experiments, the goal is to explore the relative roles and contributions of the key drivers in different scales of the PHAWL.

DATA AVAILABILITY

The DEM of the GEBCO 2022 is available at https://www.gebco.net/data_and_products/gridded_bathymetry_data/gebco_2022/. The CUDEM is available at https://coast.noaa.gov/htdata/raster2/elevation/NCEI_ninth_Topobathy_2014_8483/. The CMEMS model data can be obtained from https://resources.marine.copernicus.eu/?option=com_csw&task=results. The AVISO data is available at https://www.aviso.altimetry.fr/en/home.html. The ECMWF product can be downloaded from https://www.ecmwf.int/en/forecasts/datasets/catalogue-ecmwf-real-time-products. The HRRR data is available at https://rapidrefresh.noaa.gov/hrrr/. The dataset of NOAA stations used in this study can be downloaded from https://tidesandcurrents.noaa.gov/map/index.html. The NOAA submarine cable data can be downloaded from https://www.aoml.noaa.gov/phod/floridacurrent/data_access.php. The Argo data is available at https://nrlgodae1.nrlmry.navy.mil/cgi-bin/datalist.pl?generate=summary. The JPL-GHRSST data is available at https://podaac.jpl.nasa.gov/GHRSST. The data archive of the sensitivity experiments can be requested by e-mail to the corresponding author.

CODE AVAILABILITY

The source code of SCHISM can be accessed at https://github.com/schism-dev/schism.

Received: 27 June 2023; Accepted: 11 December 2023;
Published online: 02 January 2024

REFERENCES

1. Hoegh-Guldberg, O. et al. Impacts of 1.5 C global warming on natural and human systems (An IPCC Special Report, 2018).
2. Ceola, S., Laio, F. & Montanari, A. Satellite nighttime lights reveal increasing human exposure to floods worldwide. *Geophys. Res. Lett.* **41**, 7184–7190 (2014).
3. Ezer, T. Numerical modeling of the impact of hurricanes on ocean dynamics: sensitivity of the Gulf Stream response to storm's track. *Ocean Dyn.* **69**, 1053–1066 (2019).
4. Flather, R. A. Storm surges, pp. 2882–2892 (Encyclopedia of Ocean Science) (2001).
5. Peng, M., Xie, L. & Pietrafesa, L. J. A numerical study on hurricane-induced storm surge and inundation in Charleston Harbor, South Carolina. *J. Geophys. Res. Oceans* **111**, 22 (2006).
6. Thomas, A. et al. Influence of storm timing and forward speed on tides and storm surge during Hurricane Matthew. *Ocean Model.* **137**, 1–19 (2019).
7. Xie, L. A., Liu, H. Q., Liu, B. & Bao, S. W. A numerical study of the effect of hurricane wind asymmetry on storm surge and inundation. *Ocean Model.* **36**, 71–79 (2011).
8. Guérin, T., Bertin, X., Coulombier, T. & de Bakker, A. Impacts of wave-induced circulation in the surf zone on wave setup. *Ocean Model.* **123**, 86–97 (2018).

9. Lavaud, L., Bertin, X., Martins, K., Arnaud, G. & Bouin, M. N. The contribution of short-wave breaking to storm surges: The case Klaus in the Southern Bay of Biscay. *Ocean Model.* **156**, 14 (2020).
10. Pedreros, R. et al. Relative Contribution of Wave Setup to the Storm Surge: Observations and Modeling Based Analysis in Open and Protected Environments (Truc Vert beach and Tubuai island). *J. Coast. Res.* **85**, 1046–1050 (2018).
11. Rosenzweig, B. R. et al. Pluvial flood risk and opportunities for resilience. *Wiley Interdiscip. Rev. -Water* **5**, 18 (2018).
12. Bernhofen, M. V. et al. A first collective validation of global fluvial flood models for major floods in Nigeria and Mozambique. *Environ. Res. Lett.* **13**, 11 (2018).
13. Kirkpatrick, J. I. M. & Olbert, A. I. Modelling the effects of climate change on urban coastal-fluvial flooding. *J. Water Clim. Chang.* **11**, 270–288 (2020).
14. Ezer, T. On the interaction between a hurricane, the Gulf Stream and coastal sea level. *Ocean Dyn.* **68**, 1259–1272 (2018).
15. Park, K. et al. The contribution of hurricane remote ocean forcing to storm surge along the Southeastern US coast. *Coast. Eng.* **173**, 20 (2022).
16. Ye, F. et al. Simulating storm surge and compound flooding events with a creek-to-ocean model: Importance of baroclinic effects. *Ocean Model.* **145**, 14 (2020).
17. Moftakhari, H. R., AghaKouchak, A., Sanders, B. F., Allaire, M. & Matthew, R. A. What is nuisance flooding? Defining and monitoring an emerging challenge. *Water Resour. Res.* **54**, 4218–4227 (2018).
18. Domingues, R., Goni, G., Baringer, M. & Volkov, D. What caused the accelerated sea level changes along the us east coast during 2010-2015? *Geophys. Res. Lett.* **45**, 13367–13376 (2018).
19. Volkov, D. L., Lee, S. K., Domingues, R., Zhang, H. & Goes, M. Interannual sea level variability along the Southeastern Seaboard of the United States in relation to the Gyre-Scale heat divergence in the North Atlantic. *Geophys. Res. Lett.* **46**, 7481–7490 (2019).
20. Volkov, D. L. et al. Atlantic meridional overturning circulation increases flood risk along the United States southeast coast. *Nat. Commun.* **14**, 10 (2023).
21. Kourafalou, V. H. et al. North Atlantic Ocean OSSE system development: Nature Run evaluation and application to hurricane interaction with the Gulf Stream. *Prog. Oceanogr.* **148**, 1–25 (2016).
22. Ezer, T. & Atkinson, L. P. On the predictability of high water level along the US East Coast: can the Florida Current measurement be an indicator for flooding caused by remote forcing? *Ocean Dyn.* **67**, 751–766 (2017).
23. Ezer, T. The long-term and far-reaching impact of hurricane Dorian (2019) on the Gulf Stream and the coast. *J. Mar. Syst.* **208**, 103370 (2020).
24. Ezer, T. A modeling study of the role that bottom topography plays in Gulf Stream dynamics and in influencing the tilt of mean sea level along the US East Coast. *Ocean Dyn.* **67**, 651–664 (2017).
25. Ezer, T. Sea level rise, spatially uneven and temporally unsteady: Why the US East Coast, the global tide gauge record, and the global altimeter data show different trends. *Geophys. Res. Lett.* **40**, 5439–5444 (2013).
26. Ezer, T., Atkinson, L. P. & Tuleya, R. Observations and operational model simulations reveal the impact of Hurricane Matthew (2016) on the Gulf Stream and coastal sea level. *Dyn. Atmos. Oceans* **80**, 124–138 (2017).
27. Ezer, T., Atkinson, L. P., Corlett, W. B. & Blanco, J. L. Gulf Stream's induced sea level rise and variability along the U.S. mid-Atlantic coast. *J. Geophys. Res. Oceans* **118**, 685–697 (2013).
28. Dangendorf, S. et al. Data-driven reconstruction reveals large-scale ocean circulation control on coastal sea level. *Nat. Clim. Chang* **11**, 514 (2021).
29. Calafat, F. M., Wahl, T., Lindsten, F., Williams, J. & Frajka-Williams, E. Coherent modulation of the sea-level annual cycle in the United States by Atlantic Rossby waves. *Nat. Commun.* **9**, 13 (2018).
30. Dangendorf, S. et al. Acceleration of US Southeast and Gulf coast sea-level rise amplified by internal climate variability. *Nat. Commun.* **14**, 11 (2023).
31. Hughes, C. W. et al. Sea Level and the Role of Coastal Trapped Waves in Mediating the Influence of the Open Ocean on the Coast. *Surv. Geophys.* **40**, 1467–1492 (2019).
32. Pietrafesa, L. J. & Janowitz, G. S. Lack of evidence of southerly propagating continental-shelf waves in Onslow Bay, NC. *Geophys. Res. Lett.* **7**, 113–116 (1980).
33. Ezer, T. Can the Gulf Stream induce coherent short-term fluctuations in sea level along the US East Coast? A modeling study. *Ocean Dyn.* **66**, 207–220 (2016).
34. Pujiana, K. et al. Genesis of the Gulf Stream Subseasonal Variability in the Florida Straits. *J. Geophys. Res. Oceans* **128**, 18 (2023).
35. Chi, L. Q., Wolfe, C. L. P. & Hameed, S. Reconsidering the Relationship Between Gulf Stream Transport and Dynamic Sea Level at US East Coast. *Geophys. Res. Lett.* **50**, 10 (2023).
36. Ezer, T. Comments on "Reconsidering the Relationship Between Gulf Stream Transport and Dynamic Sea Level at US East Coast" by Chi et al. Preprint at https://essopenarchive.org/doi/full/10.22541/essoar.168626392.22220862/v1 (2023)
37. Piecuch, C. G. et al. How is New England Coastal Sea Level Related to the Atlantic Meridional Overturning Circulation at 26 degrees N? *Geophys. Res. Lett.* **46**, 5351–5360 (2019).
38. Woodworth, P. L. et al. Forcing factors affecting sea level changes at the coast. *Surv. Geophys.* **40**, 1351–1397 (2019).
39. Ponte, R. M. et al. Towards comprehensive observing and modeling systems for monitoring and predicting regional to coastal sea Level. *Front. Mar. Sci.* **6**, 25 (2019).
40. Storto, A. et al. Ocean reanalyses: recent advances and unsolved challenges. *Front. Mar. Sci.* **6**, 10 (2019).
41. Nielsen, P. *Coastal Bottom Boundary Layers And Sediment Transport*, Vol. 4 (World Scientific, 1992)
42. Piecuch, C. G. Likely weakening of the Florida Current during the past century revealed by sea-level observations. *Nat. Commun.* **11**, 13 (2020).
43. Zhang, Y. L. J. et al. Simulating compound flooding events in a hurricane. *Ocean Dyn.* **70**, 621–640 (2020).
44. Ye, F. et al. A cross-scale study for compound flooding processes during Hurricane Florence. *Nat. Hazards Earth Syst. Sci.* **21**, 1703–1719 (2021).
45. Huang, W. et al. Tidal simulation revisited. *Ocean Dyn.* **72**, 187–205 (2022).

ACKNOWLEDGEMENTS

This research is funded by the NOAA Coastal Infrastructure and Resilience Research Initiative: The Georgia Coastal Equity and Resilience (CEAR) Hub project (NA22NOS4690219).

AUTHOR CONTRIBUTIONS

K.P. conceived the idea, performed the numerical experiments and analysis, and wrote the manuscript. K.P., E.D.L., Y.J.Z., H.W., T.E., and F.Y. contributed to the discussion and editing of the manuscript. K.P., Y.J.Z., and F.Y. developed and validated the model.

COMPETING INTERESTS

The authors declare no competing interests.

ADDITIONAL INFORMATION

Supplementary information The online version contains supplementary material available at https://doi.org/10.1038/s41612-023-00549-2.

Correspondence and requests for materials should be addressed to Kyungmin Park.

Reprints and permission information is available at http://www.nature.com/reprints

Publisher's note Springer Nature remains neutral with regard to jurisdictional claims in published maps and institutional affiliations.